Chemical Control over Cellular Uptake of Organic Nanoparticles by Fine Tuning Surface Functional Groups

Yugang Bai,[⊥,†] Hang Xing,[⊥,†,‡] Peiwen Wu,[§] Xinxin Feng,[†] Kevin Hwang,[†] Jennifer M. Lee,[†] Xin Yi Phang,[†] Yi Lu,[*,†,‡,§] and Steven C. Zimmerman[*,†]

[†]Department of Chemistry, University of Illinois at Urbana—Champaign, Urbana, Illinois 61801, United States, [‡]Beckman Institute, University of Illinois at Urbana—Champaign, Urbana, Illinois 61801, United States, and [§]Department of Biochemistry, University of Illinois at Urbana—Champaign, Urbana, Illinois 61801, United States. [⊥]Y.B. and H.X. contributed equally.

ABSTRACT The functional groups displayed on the surface of nanoparticles (NP) are known to play an important role in NP cellular uptake. However, only a few systematic studies have been reported to address their role, in large part because of the difficulty in regularly varying the number and structure of the functional groups on the NP surface. We employ a bottom-up strategy for the synthesis of water-soluble organic nanoparticles (ONPs) with different sizes and functional groups, using readily available monomers. Utilizing flow cytometry, we measured the HeLa cell uptake efficiency of ONPs that contain side-chains with a different (a) length, (b) number of hydroxyl groups, and (c) number of methyl groups. We have also investigated ONPs with the same functional groups but different sizes. The potential formation and influence of protein corona was examined using the same approach but in the presence of serum. The results demonstrate that under both serum and serum-free conditions the surface-exposed functional groups determine the efficiency of cellular uptake of the particles, and that the trend can be partially predicted by the lipophilicity of the polymeric ONP's repeating units. Also, by using a "masking" strategy, these particles' cellular uptake behavior could be altered conveniently.

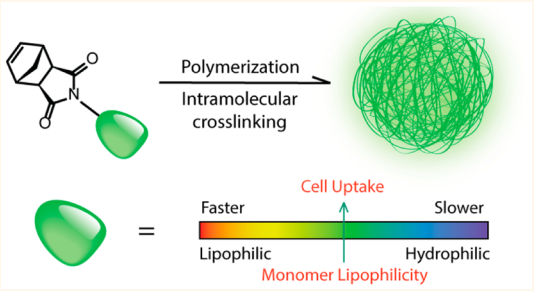

KEYWORDS: organic nanoparticle · lipophilicity · cellular uptake · surface functional groups

Nanoparticles (NPs) serve as important transport vectors for entering cells with or without desired cargo, and thus are widely applied to biological systems, especially as agents for *in vitro* and *in vivo* sensing and imaging,[1−6] drug delivery[5−12] and gene therapy.[13,14] One approach to achieve more efficient NP-mediated delivery and targeting, as well as better biocompatibility, is by tuning the functional groups on the NP surfaces. This tuning can be achieved using a wide range of surface coating methods, including ligand exchange,[15−17] PEGylation[17−19] and targeting-moiety conjugation.[17,18,20] These methods may significantly change the properties of the NPs, providing important additional desirable properties such as increased circulation time, bioderived recognition, and weakened nonspecific interactions. Appropriate and clever application of these strategies has become one of the most important elements in NP design and NP-based applications.

The mechanism by which some NPs undergo cellular internalization is critically important for their function in biomedical applications, such as drug therapy and diagnostics and, conversely, their potential toxicity.[7,21,22] Significant effort over the past decade has focused on understanding the physical, chemical, and biological interactions at the NP-biology interface.[23−26] For example, the physical and chemical properties of NPs including their size,[27−29] shape,[30−32] and surface chemistry[33−37] have been discovered to impact significantly the rate of cellular uptake.[38,39] These studies have greatly advanced our understanding of nanostructure impacts cellular uptake of NPs. However, it is generally acknowledged that these results cannot be generalized to all NPs,[39,40] and several aspects of the mechanism remain unclear because of the complexity of the process.

One key factor limiting mechanistic studies of cellular uptake is the difficulty in precisely controlling the chemistry at the

* Address correspondence to yi-lu@illinois.edu, sczimmer@illinois.edu.

Received for review June 25, 2015 and accepted September 1, 2015.

Published online September 01, 2015
10.1021/acsnano.5b03909

NP surface. Indeed, it remains very difficult to prepare model NPs wherein a single structural parameter or property is varied systematically. The most commonly studied NPs, such as metal nanoparticles (MNPs), silica nanoparticles (SiO_2—NPs) and quantum dots (QDs), often have homogeneous surfaces, and the available chemical modifications are generally limited to surface deposition and ligand exchange reactions, although mild postfunctionalization chemistries may be possible in some cases.[41] If aqueous solubility is required, highly charged or PEGylated surfaces are usually used. Likewise, the lack of reactive functional groups on their homogeneous surfaces means that traditional organic nanoparticles (ONPs)[42−45] must be prepared with similar moieties on their surfaces if water-solubility is needed. On the other hand, single-molecule polymeric ONPs, such as dendrimers,[46,47] intramolecularly cross-linked polymers[48−51] and hyperbranched polymers[52] are prepared by bottom-up synthesis, and the former two offer more flexible approaches for surface functionalization. Indeed, these macromolecules can present a controlled number of specific functional groups, designed internal structures, and narrow size distributions. In addition, polymers generally offer more ways to achieve postpolymerization modification.[53] However, the multistep preparation of dendrimers can limit the available amount of material, their size, and the range of surface functionality. Preparing ONPs from single-chain cross-linking may avoid these limitations, but to date, most ONPs prepared by this technique lack functionality or water solubility.

We recently reported a new strategy to prepare water-soluble, biocompatible ONPs using a consecutive ring-opening metathesis polymerization and ring-closing metathesis (ROMP-RCM) process.[54] The strategy allows the facile incorporation of a wide range of functional groups, synthetic scalability, and excellent size control. In continuing the study of these new ONPs, we found that the monomer used in the linear polymerization had a significant effect on the degree of cell internalization. This observation attracted our interest because this new ONP offers a particularly appealing platform for a systematic study of NP-cell interactions as a function of ONP surface properties and size (Figure 1). The bottom-up ONP synthesis not only provides a more controlled and tunable degree of functionalization, but also allows the ready integration of fluorophores to facilitate cellular uptake studies. Herein, we report how the nature of the substituents and the size of these nonionic, water-soluble ONPs affects their cellular uptake and leads to an easily controllable uptake profile different from that observed with other NPs.[38,55]

RESULTS AND DISCUSSION

We synthesized the ONPs with various functional groups by using nine different *exo*-norbornyl monomers

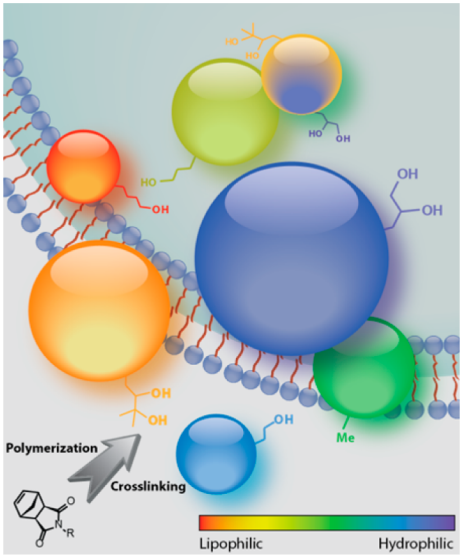

Figure 1. Schematic representation showing the use of surface functional groups to control the cellular uptake of polymeric organic nanoparticles (ONPs).

(Scheme 1), of which two monomers (M_{AE} and M_{FAM}) were used as common comonomers in all ONP preparations. The *N*-hydroxysuccinimide (HOSu) ester and fluorescein-containing monomers, M_{AE} and M_{FAM}, provided cross-linking sites and pendant fluorophores for tracking, respectively. The synthesis was straightforward and followed the general approach we reported recently (see Scheme 1 and Supporting Information).[54] Thus, the ROMP of norbornenyl derivatives mediated by Grubbs third generation catalyst allows precise control over the polymer. In particular, several physical and chemical properties of the polymer composition, length, and dispersity was easily tuned by varying the monomer to initiator ratio (M/I ratio). As noted in our previous work, careful control of the M/I ratio leads to linear polymers with molecular weights that are very close to the calculated values (Table 1 and Table S1 in Supporting Information), and each gave a low polydispersity index (PDI) as determined by gel permeation chromatography (GPC) analysis using a multiangle laser light scattering (MALLS) detector (see Figure S1 in Supporting Information). These linear poly(activated esters) with different comonomers underwent amidation with tris(allyloxymethyl)aminomethane (tri-*O*-allyl-Tris), intramolecular cross-linking *via* ring-closing metathesis (RCM), and finally dihydroxylation (and deprotection in some cases) to give well-defined ONPs, as determined by transmission electron microscopy (see Figure S2 in Supporting Information). The four most hydrophobic ONPs, ONP1, ONP3, ONP4 and ONP5, which were derived from the unprotected monomers M_{DiOH}, M_{C2OAc}, M_{C3OAc}, M_{C4OAc}, respectively, were not sufficiently soluble in pH 7.4 phosphate buffer, and were not used in the cellular uptake studies.

Before studying the cellular uptake, the cytotoxicity of ONP2 and ONP6-ONP12 was assessed. One of the

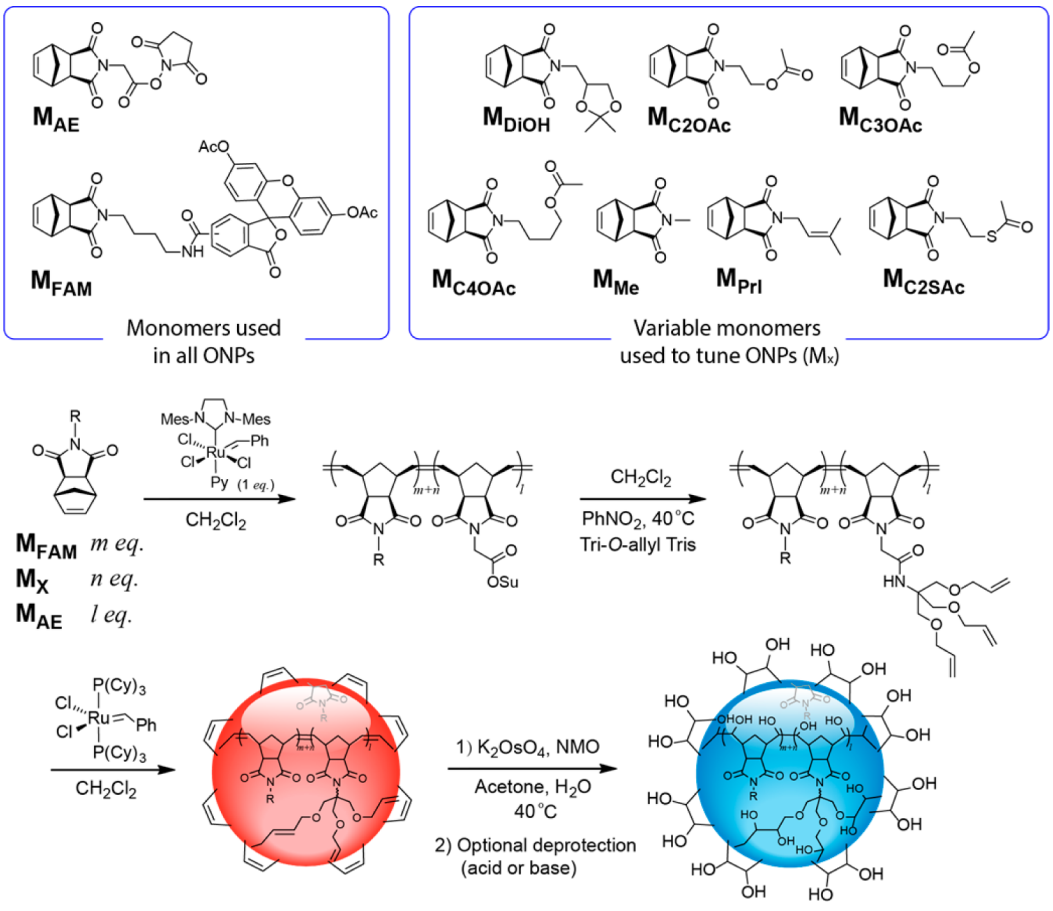

Scheme 1. Synthesis of water-soluble ONPs with different functional groups from various *exo*-norbornene derivatives. The ONP schematic is not meant to imply a particular structure. Surface is likely to be mixture of polymer chain, side-chain R-groups, and cross-linking functionality.

TABLE 1. List of Monomers and Feed Ratios of All ONPs

	feed ratio (catalyst = 1)				
ONP	M_{AE}	M_{FAM}	other monomers	deprotection	diameter (nm)[b]
ONP1	25	2	M_{DiOH} (50)	—[a]	—
ONP2	25	2	M_{DiOH} (50)	TFA	11.6
ONP3	25	2	M_{C2OAc} (50)	—	—
ONP4	25	2	M_{C3OAc} (50)	—	—
ONP5	25	2	M_{C4OAc} (50)	—	—
ONP6	25	2	M_{C2OAc} (50)	NaOH	11.8
ONP7	25	2	M_{C3OAc} (50)	NaOH	10.5
ONP8	25	2	M_{C4OAc} (50)	NaOH	11.4
ONP9	25	2	M_{Me} (50)	—	11.4
ONP10	25	2	M_{PrI} (50)	—	12.0
ONP11	25	2	M_{DiOH} (25) + M_{PrI} (25)	TFA	11.5
ONP12	25	2	M_{C2OAc} (40) + M_{C2SAc} (10)	NaOH	10.8

[a] Not deprotected. [b] Determined by DLS.

advantages of these ONPs is their comparatively low cytotoxicity, which had been established previously in HeLa cells.[55] In this study the MTT assay was applied to HepG2 cells with >80% cell viability observed for all ONPs at concentrations from 1 to 15 μM (see Figure S3 in Supporting Information). These favorably low cytotoxicity levels allowed the uptake of ONPs by HeLa cells to be examined by flow cytometry, which required a relatively high concentration of ONP (see Supporting Information for details). Because all of the ONPs had a precisely controlled degree of polymerization (DP), cross-linking density and the same fluorophore loading (two M_{AE} per polymer chain), they were approximately equal in fluorescence intensity in aqueous solutions at the same molar concentration (see Table S1 in Supporting Information). Thus, after incubating the ONPs in cell culture for a set period, the fluorescence intensity could be measured by flow cytometry and taken as proportional to the relative uptake efficiency of each ONP. The cellular uptake conditions were optimized (see details on page S32 in Supporting Information) and the uptake efficiency was evaluated by calculating an uptake index defined as

$$\text{Uptake Index} = \frac{\text{Mean } I_f \text{ of cells treated by ONPs}}{\text{Mean } I_f \text{ of untreated cells}}$$

The diameter of the ONP was clearly observed to be a key factor affecting the ONP's cellular uptake (see Figure S4 in Supporting Information), with larger particles exhibiting reduced rates of uptake. Because our interests were more focused on the role played by

surface lipophilicity, we did not investigate this behavior any further. Instead we chose six comonomers (all M_x monomers except M_{C2SAc}, Scheme 1) that cover a wide solubility range from lipophilic to hydrophilic, and display several different structural features for systematic comparison. To minimize potential differences resulting from size, we used precise control over the DP afforded by the ROMP technique to produce ONPs with similar hydrodynamic diameters. Indeed, the nine ONPs studied had an average hydrodynamic diameter of 11.4 $\pm$ 0.5 nm as determined by DLS (see Table 1 and Table S1/S2 in Supporting Information).

The most obvious comparison is between ONP6 (from M_{AE}, M_{FAM} and M_{C2OAc}), ONP7 (from M_{AE}, M_{FAM} and M_{C3OAc}) and ONP8 (from M_{AE}, M_{FAM} and M_{C4OAc}), each of which has a single hydroxyl group on alkyl side chains of increasing lengths, leading to an increasing degree of lipophilicity as follows: ONP6 < ONP7 < ONP8. These ONPs were incubated with HeLa cells for 3 h in Dulbecco's Modified Eagle Medium (DMEM) at 37 °C. The final ONP concentration of 2 μM is at the high end of the range typically used for NPs reflecting their lower toxicity (*vide supra*) and the need for a sufficient fluorescent signal. In our earlier report, we wanted to maximize cell uptake and the resultant fluorescent signal, so we used smaller ONPs (12 kDa) with four fluorescein units and worked at longer times and higher concentrations.[54] To minimize the possible impact on cell uptake from the hydrophobic fluorescein dye, in this study we used ONPs with two fluorescein monomers. Further the ONPs were larger, the concentration was lower, and the incubation time was shorter. Although the resultant increase in fluorescence signal was smaller in this uptake study, the difference was accurately quantified and showed high statistical significance using Student's *t*-test in each case (*vide infra*). The ONP-treated HeLa cells were then carefully washed and lifted for analysis by flow cytometry. As shown in Figure 2, an increase in the $-(CH_2)_n-$ linker length is accompanied by a positive (rightward) shift in the peak toward higher fluorescence intensity, indicating more efficient cellular uptake for more lipophilic NPs (Figure 2a). This trend can be more easily seen in Figure 2b, where the uptake index of the ONPs increased for the longer carbon chains on the backbone of the ONP. For example, the ONP8 showed an uptake index almost 80% higher than that of ONP6 under the same conditions.

To further examine the effect of hydrophobicity on cellular uptake of these ONPs, ONP9 (from M_{AE}, M_{FAM} and M_{Me}), ONP7 (from M_{AE}, M_{FAM} and M_{C2OAc}) and ONP2 (from M_{AE}, M_{FAM} and M_{DiOH}) were examined as a second comparison set featuring an increasing number of hydroxyl groups (0, 1, and 2). The ONP2-ONP7 comparison is particularly informative because the alkyl substituent is identical in length, differing in only the number of hydroxyl groups. Using the same

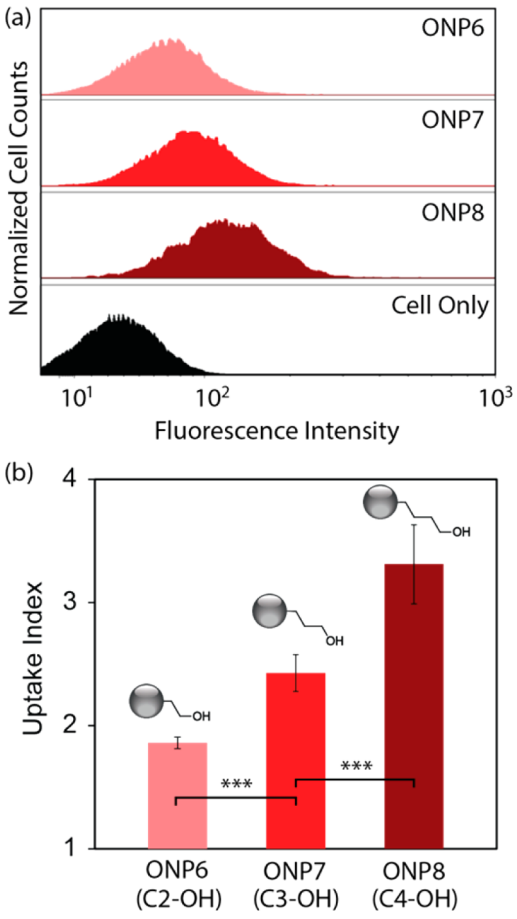

Figure 2. HeLa cellular uptake study with ONP6, ONP7 and ONP8. (a) Flow cytometry curves overlay. (b) Calculated cellular uptake indices of the three ONPs. Note: for (b), the *y*-axis starts at 1 because the uptake index cannot be lower than 1 by definition. Error bars represent standard deviation with at least three independent measurements (*$p \leq 0.001$).**

cellular uptake protocol as described above, the peak in the flow cytometer shifted to lower fluorescence intensity across the series of ONP9, ONP7, and ONP2 (Figure 3a). Thus, the uptake index of ONP9, lacking a hydroxyl group, was clearly higher than that of ONP7 with one hydroxyl group, which, in turn, was higher than the uptake index of ONP2 with two hydroxyl groups per side chain (Figure 3b). The results are consistent with the previous finding that ONPs with more hydrophobic domains are more readily taken up by cells.

A special advantage of this bottom-up strategy is illustrated by the third set of ONPs. In particular, the ROMP-RCM strategy used in this work allows a nearly unlimited degree of fine-tuning because two or more functional monomers can be randomly copolymerized at any feed ratio to provide a desired property with high precision. To illustrate this broad concept, ONP11 was synthesized from M_{AE}, M_{DiOH}, M_{PrI}, and M_{FAM} with feed ratio of 25:25:25:2, respectively, representing a 1:1 blend of the monomers used to prepare ONP2 (from M_{AE}, M_{FAM} and M_{DiOH}) and ONP10 (from M_{AE}, M_{FAM} and M_{PrI}), and it was characterized similarly by flow

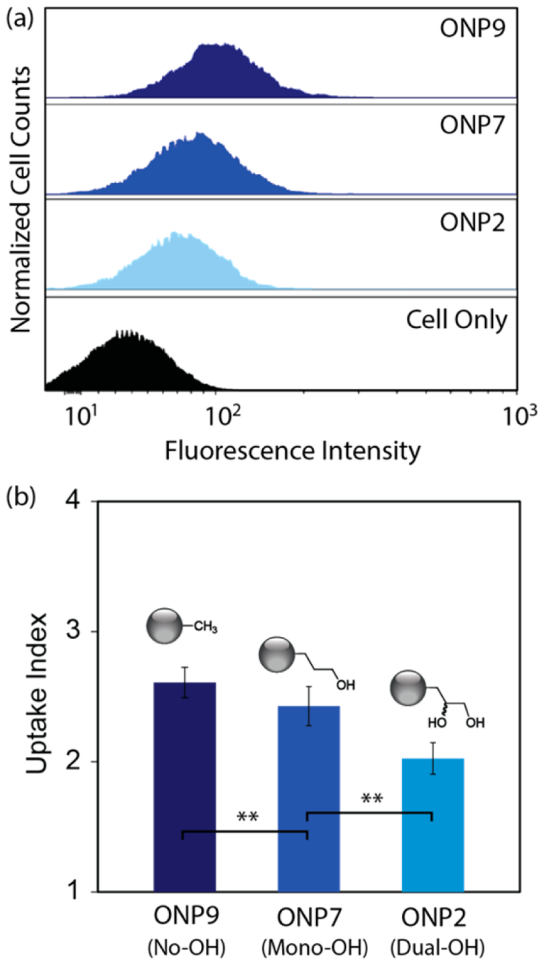

Figure 3. HeLa cellular uptake study with ONP9, ONP7 and ONP2. (a) Flow cytometry curves overlay. (b) Calculated cellular uptake indices of the three ONPs. Error bars represent standard deviation with at least three independent measurements ($p \leq 0.01$).**

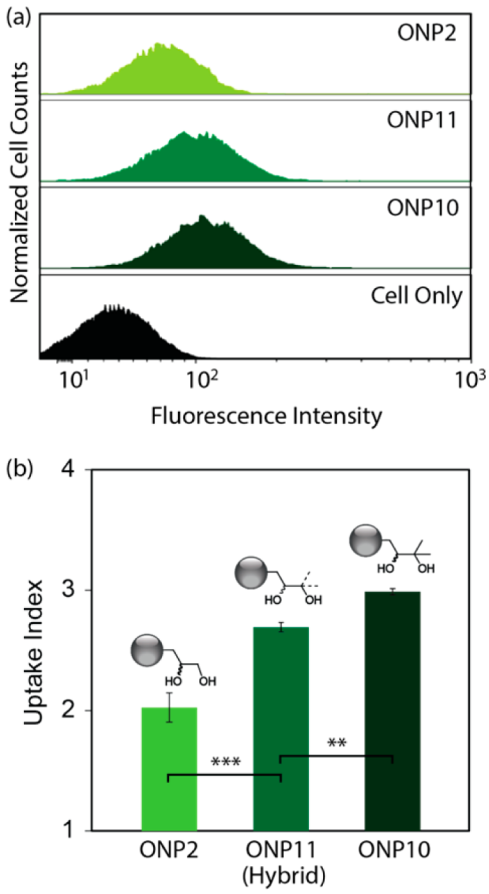

Figure 4. HeLa cellular uptake study with ONP2, ONP10 and ONP11. (a) Flow cytometry curves overlay. (b) Calculated cellular uptake indices of the three ONPs. Error bars represent standard deviation with at least three independent measurements ($p \leq 0.01$; ***$p \leq 0.001$).**

cytometry. As seen in Figure 4, ONP10 showed the highest, ONP2 the lowest, and "hybrid" ONP11 an intermediate uptake index. This result is important, because it indicates that an averaged NP internalization profile may be obtained by combining two other internalization profiles with mixed monomers in linear polymer synthesis. This approach may eliminate the need to synthesize and test additional monomers for optimized delivery properties, and allow for predictable, fine-tuning of ONP uptake properties.

Although we have demonstrated that the cellular uptake capability of ONPs can be tuned by surface functional groups and sizes in serum-free condition, the mechanism for ONP uptake is still unclear. Previous studies on ONP cellular uptake suggest that in natural biological environments, a protein corona can form on the surface of the NPs, and play a central role in determining nanoparticle behavior.[29,37,56−60] The corona formation on the nanoparticle surface can be reversible or irreversible.[55,61−63] Our findings which indicate that more lipophilic NPs lead to higher cellular uptake are consistent many prior studies that found the same trend with metal NPs under serum-free conditions (no corona formation).[64,65] The trend can sometimes be completely reversed in the presence of serum because the more hydrophobic NPs tend to absorb more protein, significantly reducing NP internalization.[35,66,67] In a very recent report, Rotello and co-workers showed that AuNPs coated with zwitterionic groups do not form hard corona and exhibit the same internalization trend as NPs in serum-free conditions.[55] This important finding showed the possibility of using the presentation of chemical functionality to control the NP cellular uptake under physiological condition.

To determine the influence of serum on the cellular uptake of the ONPs investigated here, the uptake studies with all the previously tested ONPs were determined after the ONPs were incubated with HeLa cells in DMEM medium with 10% fetal bovine serum (FBS). The flow cytometry results showed that cells treated with ONP8 (with the longest alkane linker), ONP9 (with no hydroxyl group) and ONP10 (with the most methyl groups) exhibited the highest fluorescent intensity among each group, following the same trend

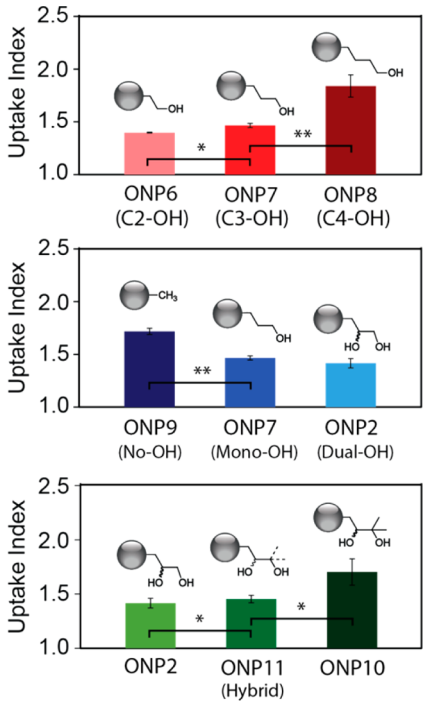

Figure 5. Uptake indices of the three sets of ONPs from repeated HeLa cellular uptake studies with 10% FBS. ONPs showed the same trend in these studies as they did under serum-free conditions. Error bars represent standard deviation with at least three independent measurements (*$p \leq 0.05$; **$p \leq 0.01$).

seen in serum-free medium (Figure 5 and Figure S5 in Supporting Information). The overall uptake efficiency with 10% FBS was lower compared to the studies of "naked" NPs under serum-free conditions, consistent with previously reported results.[55,59,68−71] However, the key finding is that we observed only an attenuation of uptake, not a reversal of uptake rates with the more hydrophobic ONPs.

The hydroxyl-rich, neutral nature (see Table S2 in Supporting Information) of the cross-linked ONPs was anticipated to confer biocompatibility and resist forming an irreversible corona with serum treatment.[55,71,72] Verifying directly the presence or absence of a corona is difficult because of the low density of our ONPs,[54] however, we could confirm by dynamic light scattering (DLS) the absence of significantly larger ONP-protein or ONP-ONP aggregates in a mixture of ONP2 and 10% FBS (see Figure S6 in Supporting Information). Thus, although we are not able to determine definitively the origin of the uptake attenuation observed in serum, it is important to note that some degree of lipophilicity tuning continues to be effective in serum. At least one ONP in this more physiologically relevant media could exhibit comparable uptake efficiency to a "naked" ONP.

Two limiting mechanisms for NP cellular uptake have been proposed, which involve passive diffusion across the cell membrane, and semispecific interactions between NP surface functional groups and the cell surface, the latter leading to receptor-mediated internalization. To obtain evidence that might distinguish these possibilities, we repeated the flow cytometry experiments at lower temperature (4 °C), where cell surface receptor-mediated internalization is dramatically suppressed.[73−76] As shown in Figure S7 (see Supporting Information), at 4 °C, almost no uptake was observed, suggesting that the ONPs may have entered HeLa cells mainly through a receptor-mediated internalization process, instead of by passive permeation.[54] However, this preliminary observation requires further investigation before a detailed mechanism can be assigned.[77]

The analysis of lipophilicity above was based on pairwise comparisons of structurally similar monomers. With the goal of comparing all of the monomers at once in a more systematic way, we wondered if the lipophilicity of the ONP constituent monomer units could be quantified. Such a scale might be used to predict the cellular uptake efficiency of ONPs from the more readily prepared repeating units, avoiding the lengthier ONP preparation. Thus, to determine the relative lipophilicity of the variable repeating units in the ONPs semiquantitatively, these interchangeable monomers were dihydroxylated under Upjohn conditions and deprotected when necessary, affording a total of ten repeating unit mimics (RUMs, labeled RUM1−RUM10, Figure 6). These compounds were easily prepared and were used without separating possible stereoisomeric products (see Figure 7). The retention time t of each compound (RUM1-RUM10) in a reverse-phase LC-MS system was taken as a relative measure of the repeating unit's lipophilicity and it was assumed to correlate with that of the corresponding ONP surface (see Figure 7 and additional information in Figure S8 and Table S4 in Supporting Information). For ONP11 containing two monomers in a 1:1 ratio, a virtual t was calculated as an average from the t of the two corresponding RUMs: $t_{avg} = 10^{[(\log t_1 + \log t_2)/2]}$. This relationship arose from the direct correlation between LC retention time and partition coefficient P.[78] These RUMs covered a wide lipophilicity range, with RUM2 being the most hydrophilic and RUM5 being the most lipophilic.

In examining the RUM retention time t *vs* uptake index correlation in Figure 7, one sees at the broadest level a general trend that more lipophilic ONPs entering cells more easily. This correlation holds both in serum and under serum-free conditions. However, because the cellular uptake of NPs is a complicated process, especially in serum, and might be influenced by many factors other than NP lipophilicity and size, deviations from this general trend are observed. For example, in 10% FBS, the most hydrophilic ONP2 showed slightly higher uptake than the less hydrophilic ONP6. In addition, RUM7 and RUM9 had extremely close retention times, yet ONP7 exhibited a smaller uptake index compared to ONP9. These minor variations in the

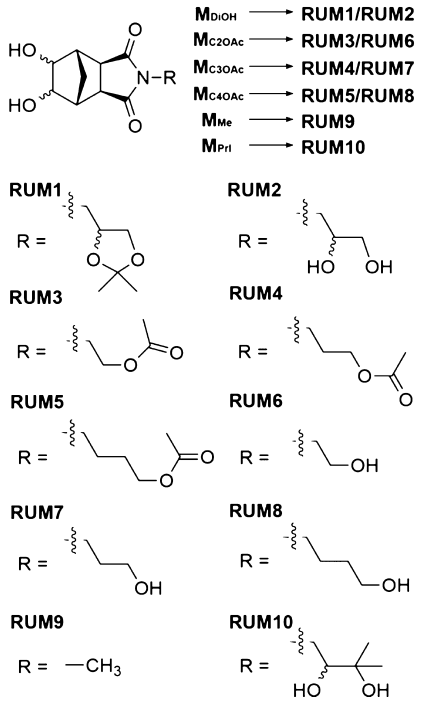

Figure 6. Structure of "repeating unit mimics" (RUMs) that resembles the functional repeating units within the ONP scaffolds. For easy comparison, these mimics have the same numbering as their corresponding ONPs (*e.g.*, ONP1 has the repeating units analogous to RUM1).

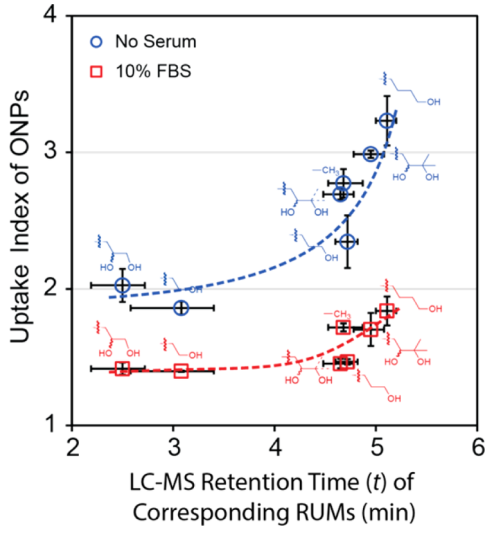

Figure 7. Illustration of the relationship between ONP cellular uptake efficiency and their corresponding repeating units in serum-free (blue) or with 10% FBS (red) conditions. Lipophilicity of the repeating units was represented as the LC–MS retention time of the corresponding RUM. The dashed curves are added to assist visual assessment of the trends.

overall uptake trends may suggest a complicated NP cellular uptake process, which could be influenced by many factors other than NP lipophilicity and size.

A high level of predictability in NP cellular uptake efficiencies was shown to be possible when the protein corona fingerprint is determined.[37] Nonetheless, the LC retention time of RUMs serves as a quantitative

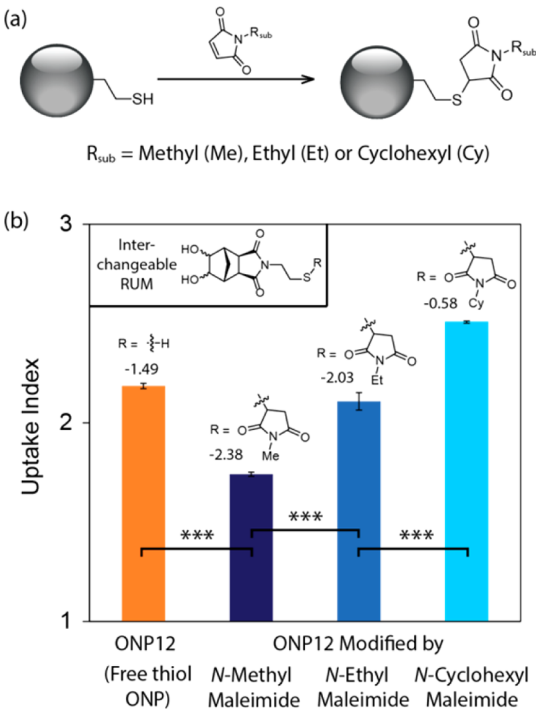

Figure 8. (a) Schematic illustration of the ONP maleimide-masking strategy using a thiol-bearing ONP12 (10 -SH groups per ONP on average). (b) Uptake index comparison of the unmasked ONP12 and the resulting maleimide-masked ONPs from it. The numbers above the bars were calculated log *P* values (Marvin Beans version 15.6.1, ChemAxon Ltd.) of the masked (by maleimides) or unmasked (free thiol) RUMs. Log *P* values were used because RUMs could not be easily prepared for the thiol monomer. More lipophilic maleimide led to more lipophilic RUM, giving higher uptake index of the corresponding ONP. Error bars represent standard deviation with at least three independent measurements (*$p \leq 0.001$).**

experimental parameter that can approximate the cellular uptake efficiency of the ONPs examined here. In particular, the uptake efficiency in serum-free conditions responded minimally to the lipophilicity increase of surface functionalities when the ONP was more hydrophilic ($t <$ *ca.* 4.7 min), but increased dramatically with increases in hydrophobicity for monomers whose corresponding t were more than 4.7 min. Moreover, in the presence of 10% FBS, a similar trend was observed, but with both the overall trend and uptake efficiencies attenuated. This analysis not only allows the properties of ONPs to be estimated from mixed monomers, it also suggests a potential approach for rational design of ONPs with tunable properties. Most importantly, it is clear that the functional groups on the ONP surface were still actively altering the ONP cellular uptake behavior even in the presence of serum proteins.

It is worth noting that RUM2, RUM6, RUM7 and RUM8 are the unmasked (deprotected) product of RUM1, RUM3, RUM4 and RUM5. Such hydrophobic–hydrophilic pairs can be used to prepare ONPs with tunable cellular uptake properties using an "on-demand unmasking," as exemplified in the synthesis of ONP11.

To further demonstrate the concept of "masked" *versus* "unmasked" ONPs with predictable changes in cellular uptake, a new thiol-bearing ONP12 (from M_{AE}, M_{FAM}, M_{C2OAc} and M_{C2SAc}, 25:2:40:10) was synthesized. The thiol groups on this ONP were conveniently masked using bioorthogonal thiol-maleimide conjugation chemistry, with *N*-methylmaleimide, *N*-ethylmaleimide or *N*-cyclohexylmaleimide. The masked ONPs were evaluated by flow cytometry, and the results were shown in Figure 8 and Figure S9 in Supporting Information.

On average, ONP12 had 10 hydroxyl groups replaced with the more lipophilic thiol groups compared to ONP6, and as predicted, it showed a higher uptake index compared to ONP6. By modifying the thiol-ONP with three different maleimides, three new ONPs with varied surface lipophilicity were obtained. Based on the lipophilicity of the masking maleimide, the new ONP showed a decrease or increase in its uptake index. In particular, the water-soluble, very hydrophilic *N*-methylmaleimide decreased the ONP's uptake index considerably upon Michael addition mediated masking, whereas the strongly hydrophobic *N*-cyclohexylmaleimide clearly facilitated the uptake process. Despite being a relatively simple model, this example shows the potential of utilizing masked-unmasked ONP pairs with predictable changes in cellular uptake.

CONCLUSION

In summary, we have demonstrated that the lipophilicity of polymeric ONPs prepared using a new ROMP-RCM strategy were facilely tuned by using different monomers, and that this in turn significantly altered their cellular uptake profile with HeLa cells. With an increase in repeating unit lipophilicity or a decrease of ONP size, the cell internalization rate of the corresponding ONP increased. In serum-containing biological environments, these ONPs could still show improved cellular uptake efficiency as the particle lipophilicity increased, similar to the trend observed for many of the NPs in buffered solution. The use of different monomers combined with the ability to freely adjust their feed ratios offers the possibility to fine-tune the ONP-cell interactions directly or through an "on-demand" approach. The concept of "masked" *versus* "unmasked" ONPs was demonstrated using a thiol-bearing ONP that underwent predictable changes in cellular uptake upon maleimide conjugation. Although more general conclusions about other cell lines (*i.e.*, beyond HeLa cells) and concentrations cannot be made at this time, our observations and findings do show the potential of the ROMP-RCM strategy to create promising scaffolds for functional, tunable, and biocompatible delivery vehicles.

METHODS

Synthesis of ONPs. ONPs were synthesized from living polymerization of the corresponding monomers, functionalized by tri-*O*-allyl-Tris, intramolecularly cross-linked by RCM, and finally dihydroxylated and deprotected if necessary. Detailed procedures for each step (polymerization, allylation, RCM and dihydroxylation) can be found in the Supporting Information.

Cellular Uptake Study. HeLa cells used for ONP uptake experiments were cultured in Dulbecco's modification of Eagle's medium (DMEM) supplemented with or without 10% Fetal Bovine Serum (FBS), 100 U/mL penicillin, and 100 μg/mL streptomycin, on 25 cm^2 culture flasks in a humidified 5% CO_2 incubator at 37 °C. HeLa cells were plated onto 35 mm glass-bottom dishes (MatTek) and grown to 70−90% confluence before experiments. HeLa cells were then incubated with 2 mL of DMEM (with or without 10% FBS) containing ONPs (2 μM) in glass-bottom dish. After 3 h, cells were washed with PBS 3 times and fresh DMEM (with or without 10% FBS) was added. For flow cytometry study, after the 3 h incubation with ONPs, HeLa cells were washed with PBS and detached by 0.05% trypsin. The suspended cell solution was collected by centrifugation at 2000 *g* for 5 min and further washed with PBS three times. Flow cytometry was performed using a BD FACSCanto system under 488 nm excitation. Control cells without any treatment were used to set the gating. Each measurement set was performed using 10 000 cells.

Synthesis of Monomers and RUMs. All the synthetic procedures for the monomers and RUMs, as well as additional characterization details are included in the Supporting Information.

Conflict of Interest: The authors declare no competing financial interest.

Acknowledgment. The authors are gratefully thankful for the funding from the Binational Science Foundation (2010047), the National Science Foundation (CHE-1307404), the U.S. National Institutes of Health (Grant ES016865), and the funding by the Office of Science (BER), the U.S. Department of Energy (DE-FG02-08ER64568).

Supporting Information Available: The Supporting Information is available free of charge on the ACS Publications website at DOI: 10.1021/acsnano.5b03909.

Experimental details for the material preparation, characterization, and testing. (PDF)

REFERENCES AND NOTES

1. De, M.; Ghosh, P. S.; Rotello, V. M. Applications of Nanoparticles in Biology. *Adv. Mater.* **2008**, *20*, 4225–4241.
2. Yang, S. K.; Shi, X.; Park, S.; Ha, T.; Zimmerman, S. C. A Dendritic Single-Molecule Fluorescent Probe That Is Monovalent, Photostable and Minimally Blinking. *Nat. Chem.* **2013**, *5*, 692–697.
3. Yin, Q.; Yap, F. Y.; Yin, L.; Ma, L.; Zhou, Q.; Dobrucki, L. W.; Fan, T. M.; Gaba, R. C.; Cheng, J. Poly(Iohexol) Nanoparticles as Contrast Agents for in Vivo X-Ray Computed Tomography Imaging. *J. Am. Chem. Soc.* **2013**, *135*, 13620–13623.
4. Qian, X.; Peng, X.-H.; Ansari, D. O.; Yin-Goen, Q.; Chen, G. Z.; Shin, D. M.; Yang, L.; Young, A. N.; Wang, M. D.; Nie, S. In Vivo Tumor Targeting and Spectroscopic Detection with Surface-Enhanced Raman Nanoparticle Tags. *Nat. Biotechnol.* **2008**, *26*, 83–90.
5. Jiang, S.; Win, K. Y.; Liu, S.; Teng, C. P.; Zheng, Y.; Han, M.-Y. Surface-Functionalized Nanoparticles for Biosensing and Imaging-Guided Therapeutics. *Nanoscale* **2013**, *5*, 3127–3148.
6. Dreaden, E. C.; Alkilany, A. M.; Huang, X.; Murphy, C. J.; El-Sayed, M. A. The Golden Age: Gold Nanoparticles for Biomedicine. *Chem. Soc. Rev.* **2012**, *41*, 2740–2779.
7. Davis, M. E.; Chen, Z.; Shin, D. M. Nanoparticle Therapeutics: An Emerging Treatment Modality for Cancer. *Nat. Rev. Drug Discovery* **2008**, *7*, 771–782.

8. Liong, M.; Lu, J.; Kovochich, M.; Xia, T.; Ruehm, S. G.; Nel, A. E.; Tamanoi, F.; Zink, J. I. Multifunctional Inorganic Nanoparticles for Imaging, Targeting, and Drug Delivery. *ACS Nano* **2008**, *2*, 889–896.
9. Cho, K. J.; Wang, X.; Nie, S. M.; Chen, Z.; Shin, D. M. Therapeutic Nanoparticles for Drug Delivery in Cancer. *Clin. Cancer Res.* **2008**, *14*, 1310–1316.
10. Gao, X.; Cui, Y.; Levenson, R. M.; Chung, L. W. K.; Nie, S. In Vivo Cancer Targeting and Imaging with Semiconductor Quantum Dots. *Nat. Biotechnol.* **2004**, *22*, 969–976.
11. Poon, Z.; Chang, D.; Zhao, X.; Hammond, P. T. Layer-by-Layer Nanoparticles with a Ph-Sheddable Layer for in Vivo Targeting of Tumor Hypoxia. *ACS Nano* **2011**, *5*, 4284–4292.
12. Lai, J.; Shah, B. P.; Garfunkel, E.; Lee, K.-B. Versatile Fluorescence Resonance Energy Transfer-Based Mesoporous Silica Nanoparticles for Real-Time Monitoring of Drug Release. *ACS Nano* **2013**, *7*, 2741–2750.
13. Mastrobattista, E.; van der Aa, M. A. E. M.; Hennink, W. E.; Crommelin, D. J. A. Artificial Viruses: A Nanotechnological Approach to Gene Delivery. *Nat. Rev. Drug Discovery* **2006**, *5*, 115–121.
14. Kogure, K.; Akita, H.; Yamada, Y.; Harashima, H. Multifunctional Envelope-Type Nano Device (Mend) as a Non-Viral Gene Delivery System. *Adv. Drug Delivery Rev.* **2008**, *60*, 559–571.
15. Duan, H.; Nie, S. Cell-Penetrating Quantum Dots Based on Multivalent and Endosome-Disrupting Surface Coatings. *J. Am. Chem. Soc.* **2007**, *129*, 3333–3338.
16. Latham, A. H.; Williams, M. E. Controlling Transport and Chemical Functionality of Magnetic Nanoparticles. *Acc. Chem. Res.* **2008**, *41*, 411–420.
17. Susumu, K.; Uyeda, H. T.; Medintz, I. L.; Pons, T.; Delehanty, J. B.; Mattoussi, H. Enhancing the Stability and Biological Functionalities of Quantum Dots *via* Compact Multifunctional Ligands. *J. Am. Chem. Soc.* **2007**, *129*, 13987–13996.
18. Oh, E.; Delehanty, J. B.; Sapsford, K. E.; Susumu, K.; Goswami, R.; Blanco-Canosa, J. B.; Dawson, P. E.; Granek, J.; Shoff, M.; Zhang, Q.; Goering, P. L.; Huston, A.; Medintz, I. L. Cellular Uptake and Fate of Pegylated Gold Nanoparticles Is Dependent on Both Cell-Penetration Peptides and Particle Size. *ACS Nano* **2011**, *5*, 6434–6448.
19. Jokerst, J. V.; Lobovkina, T.; Zare, R. N.; Gambhir, S. S. Nanoparticle Pegylation for Imaging and Therapy. *Nanomedicine* **2011**, *6*, 715–728.
20. Wu, X. A.; Choi, C. H. J.; Zhang, C.; Hao, L.; Mirkin, C. A. Intracellular Fate of Spherical Nucleic Acid Nanoparticle Conjugates. *J. Am. Chem. Soc.* **2014**, *136*, 7726–7733.
21. Canton, I.; Battaglia, G. Endocytosis at the Nanoscale. *Chem. Soc. Rev.* **2012**, *41*, 2718–2739.
22. Kim, S. T.; Saha, K.; Kim, C.; Rotello, V. M. The Role of Surface Functionality in Determining Nanoparticle Cytotoxicity. *Acc. Chem. Res.* **2013**, *46*, 681–691.
23. Mahon, E.; Salvati, A.; Bombelli, F. B.; Lynch, I.; Dawson, K. A. Designing the Nanoparticle-Biomolecule Interface for "Targeting and Therapeutic Delivery". *J. Controlled Release* **2012**, *161*, 164–174.
24. Nel, A. E.; Madler, L.; Velegol, D.; Xia, T.; Hoek, E. M. V.; Somasundaran, P.; Klaessig, F.; Castranova, V.; Thompson, M. Understanding Biophysicochemical Interactions at the Nano-Bio Interface. *Nat. Mater.* **2009**, *8*, 543–557.
25. Chou, L. Y. T.; Ming, K.; Chan, W. C. W. Strategies for the Intracellular Delivery of Nanoparticles. *Chem. Soc. Rev.* **2011**, *40*, 233–245.
26. Walkey, C. D.; Chan, W. C. W. Understanding and Controlling the Interaction of Nanomaterials with Proteins in a Physiological Environment. *Chem. Soc. Rev.* **2012**, *41*, 2780–2799.
27. Tang, L.; Yang, X.; Yin, Q.; Cai, K.; Wang, H.; Chaudhury, I.; Yao, C.; Zhou, Q.; Kwon, M.; Hartman, J. A.; Dobrucki, I. T.; Dobrucki, L. W.; Borst, L. B.; Lezmi, S.; Helferich, W. G.; Ferguson, A. L.; Fan, T. M.; Cheng, J. Investigating the Optimal Size of Anticancer Nanomedicine. *Proc. Natl. Acad. Sci. U. S. A.* **2014**, *111*, 15344–15349.
28. Jiang, W.; Kim, B. Y. S.; Rutka, J. T.; Chan, W. C. W. Nanoparticle-Mediated Cellular Response Is Size-Dependent. *Nat. Nanotechnol.* **2008**, *3*, 145–150.
29. Walkey, C. D.; Olsen, J. B.; Guo, H. B.; Emili, A.; Chan, W. C. W. Nanoparticle Size and Surface Chemistry Determine Serum Protein Adsorption and Macrophage Uptake. *J. Am. Chem. Soc.* **2012**, *134*, 2139–2147.
30. Barua, S.; Yoo, J. W.; Kolhar, P.; Wakankar, A.; Gokarn, Y. R.; Mitragotri, S. Particle Shape Enhances Specificity of Antibody-Displaying Nanoparticles. *Proc. Natl. Acad. Sci. U. S. A.* **2013**, *110*, 3270–3275.
31. Huang, X. L.; Teng, X.; Chen, D.; Tang, F. Q.; He, J. Q. The Effect of the Shape of Mesoporous Silica Nanoparticles on Cellular Uptake and Cell Function. *Biomaterials* **2010**, *31*, 438–448.
32. Zhang, K.; Fang, H. F.; Chen, Z. Y.; Taylor, J. S. A.; Wooley, K. L. Shape Effects of Nanoparticles Conjugated with Cell-Penetrating Peptides (Hiv Tat Ptd) on Cho Cell Uptake. *Bioconjugate Chem.* **2008**, *19*, 1880–1887.
33. Hu, Y.; Xie, J. W.; Tong, Y. W.; Wang, C. H. Effect of Peg Conformation and Particle Size on the Cellular Uptake Efficiency of Nanoparticles with the Hepg2 Cells. *J. Controlled Release* **2007**, *118*, 7–17.
34. Hauck, T. S.; Ghazani, A. A.; Chan, W. C. W. Assessing the Effect of Surface Chemistry on Gold Nanorod Uptake, Toxicity, and Gene Expression in Mammalian Cells. *Small* **2008**, *4*, 153–159.
35. Patil, S.; Sandberg, A.; Heckert, E.; Self, W.; Seal, S. Protein Adsorption and Cellular Uptake of Cerium Oxide Nanoparticles as a Function of Zeta Potential. *Biomaterials* **2007**, *28*, 4600–4607.
36. Dai, Q.; Walkey, C.; Chan, W. C. W. Polyethylene Glycol Backfilling Mitigates the Negative Impact of the Protein Corona on Nanoparticle Cell Targeting. *Angew. Chem., Int. Ed.* **2014**, *53*, 5093–5096.
37. Walkey, C. D.; Olsen, J. B.; Song, F.; Liu, R.; Guo, H.; Olsen, D. W. H.; Cohen, Y.; Emili, A.; Chan, W. C. W. Protein Corona Fingerprinting Predicts the Cellular Interaction of Gold and Silver Nanoparticles. *ACS Nano* **2014**, *8*, 2439–2455.
38. Chithrani, B. D.; Ghazani, A. A.; Chan, W. C. W. Determining the Size and Shape Dependence of Gold Nanoparticle Uptake into Mammalian Cells. *Nano Lett.* **2006**, *6*, 662–668.
39. Albanese, A.; Tang, P. S.; Chan, W. C. W. The Effect of Nanoparticle Size, Shape, and Surface Chemistry on Biological Systems. *Annu. Rev. Biomed. Eng.* **2012**, *14*, 1–16.
40. Rivera-Gil, P.; Jimenez De Aberasturi, D.; Wulf, V.; Pelaz, B.; Del Pino, P.; Zhao, Y.; De La Fuente, J. M.; Ruiz De Larramendi, I.; Rojo, T.; Liang, X.-J.; Parak, W. J. The Challenge to Relate the Physicochemical Properties of Colloidal Nanoparticles to Their Cytotoxicity. *Acc. Chem. Res.* **2013**, *46*, 743–749.
41. Balasubramanian, R.; Kwon, Y.-G.; Wei, A. Encapsulation and Functionalization of Nanoparticles in Crosslinked Resorcinarene Shells. *J. Mater. Chem.* **2007**, *17*, 105–112.
42. Mora-Huertas, C. E.; Fessi, H.; Elaissari, A. Polymer-Based Nanocapsules for Drug Delivery. *Int. J. Pharm.* **2010**, *385*, 113–142.
43. Johnson, J. A.; Lu, Y. Y.; Burts, A. O.; Lim, Y.-H.; Finn, M. G.; Koberstein, J. T.; Turro, N. J.; Tirrell, D. A.; Grubbs, R. H. Core-Clickable Peg-Branch-Azide Bivalent-Bottle-Brush Polymers by Romp: Grafting-through and Clicking-To. *J. Am. Chem. Soc.* **2010**, *133*, 559–566.
44. Liu, J.; Burts, A. O.; Li, Y.; Zhukhovitskiy, A. V.; Ottaviani, M. F.; Turro, N. J.; Johnson, J. A. Brush-First" Method for the Parallel Synthesis of Photocleavable, Nitroxide-Labeled Poly(Ethylene Glycol) Star Polymers. *J. Am. Chem. Soc.* **2012**, *134*, 16337–16344.
45. Carrillo, A.; Yanjarappa, M. J.; Gujraty, K. V.; Kane, R. S. Biofunctionalized Block Copolymer Nanoparticles Based on Ring-Opening Metathesis Polymerization. *J. Polym. Sci., Part A: Polym. Chem.* **2006**, *44*, 928–939.
46. Vögtle, F.; Gestermann, S.; Hesse, R.; Schwierz, H.; Windisch, B. Functional Dendrimers. *Prog. Polym. Sci.* **2000**, *25*, 987–1041.

47. Hecht, S. Functionalizing the Interior of Dendrimers: Synthetic Challenges and Applications. *J. Polym. Sci., Part A: Polym. Chem.* **2003**, *41*, 1047–1058.
48. Harth, E.; Horn, B. V.; Lee, V. Y.; Germack, D. S.; Gonzales, C. P.; Miller, R. D.; Hawker, C. J. A Facile Approach to Architecturally Defined Nanoparticles *via* Intramolecular Chain Collapse. *J. Am. Chem. Soc.* **2002**, *124*, 8653–8660.
49. Cherian, A. E.; Sun, F. C.; Sheiko, S. S.; Coates, G. W. Formation of Nanoparticles by Intramolecular Cross-Linking: Following the Reaction Progress of Single Polymer Chains by Atomic Force Microscopy. *J. Am. Chem. Soc.* **2007**, *129*, 11350–11351.
50. Foster, E. J.; Berda, E. B.; Meijer, E. W. Metastable Supramolecular Polymer Nanoparticles *via* Intramolecular Collapse of Single Polymer Chains. *J. Am. Chem. Soc.* **2009**, *131*, 6964–6966.
51. Ouchi, M.; Badi, N.; Lutz, J.-F.; Sawamoto, M. Single-Chain Technology Using Discrete Synthetic Macromolecules. *Nat. Chem.* **2011**, *3*, 917–924.
52. Wilms, D.; Stiriba, S.-E.; Frey, H. Hyperbranched Polyglycerols: From the Controlled Synthesis of Biocompatible Polyether Polyols to Multipurpose Applications. *Acc. Chem. Res.* **2009**, *43*, 129–141.
53. Theato, P.; Klok, H.-A. *Functional Polymers by Post-Polymerization Modification: Concepts, Guidelines, and Applications*; Wiley-VCH Verlag GmbH & Co. KgaA: Weinheim, 2013.
54. Bai, Y.; Xing, H.; Vincil, G. A.; Lee, J.; Henderson, E. J.; Lu, Y.; Lemcoff, N. G.; Zimmerman, S. C. Practical Synthesis of Water-Soluble Organic Nanoparticles with a Single Reactive Group and a Functional Carrier Scaffold. *Chem. Sci.* **2014**, *5*, 2862–2868.
55. Moyano, D. F.; Saha, K.; Prakash, G.; Yan, B.; Kong, H.; Yazdani, M.; Rotello, V. M. Fabrication of Corona-Free Nanoparticles with Tunable Hydrophobicity. *ACS Nano* **2014**, *8*, 6748–6755.
56. Cedervall, T.; Lynch, I.; Lindman, S.; Berggård, T.; Thulin, E.; Nilsson, H.; Dawson, K. A.; Linse, S. Understanding the Nanoparticle-Protein Corona Using Methods to Quantify Exchange Rates and Affinities of Proteins for Nanoparticles. *Proc. Natl. Acad. Sci. U. S. A.* **2007**, *104*, 2050–2055.
57. Lundqvist, M.; Stigler, J.; Cedervall, T.; Berggård, T.; Flanagan, M. B.; Lynch, I.; Elia, G.; Dawson, K. The Evolution of the Protein Corona around Nanoparticles: A Test Study. *ACS Nano* **2011**, *5*, 7503–7509.
58. Fleischer, C. C.; Payne, C. K. Nanoparticle−Cell Interactions: Molecular Structure of the Protein Corona and Cellular Outcomes. *Acc. Chem. Res.* **2014**, *47*, 2651–2659.
59. Pelaz, B.; del Pino, P.; Maffre, P.; Hartmann, R.; Gallego, M.; Rivera-Fernández, S.; de la Fuente, J. M.; Nienhaus, G. U.; Parak, W. J. Surface Functionalization of Nanoparticles with Polyethylene Glycol: Effects on Protein Adsorption and Cellular Uptake. *ACS Nano* **2015**, *9*, 6996–7008.
60. Pino, P. d.; Pelaz, B.; Zhang, Q.; Maffre, P.; Nienhaus, G. U.; Parak, W. J. Protein Corona Formation around Nanoparticles - from the Past to the Future. *Mater. Horiz.* **2014**, *1*, 301–313.
61. Milani, S.; Baldelli Bombelli, F.; Pitek, A. S.; Dawson, K. A.; Rädler, J. Reversible *versus* Irreversible Binding of Transferrin to Polystyrene Nanoparticles: Soft and Hard Corona. *ACS Nano* **2012**, *6*, 2532–2541.
62. Casals, E.; Puntes, V. F. Inorganic Nanoparticle Biomolecular Corona: Formation, Evolution and Biological Impact. *Nanomedicine* **2012**, *7*, 1917–1930.
63. Monopoli, M. P.; Pitek, A. S.; Lynch, I.; Dawson, K. A. Formation and Characterization of the Nanoparticle-Protein Corona. *Methods Mol. Biol.* **2013**, *1025*, 137–155.
64. Zhu, Z.-J.; Posati, T.; Moyano, D. F.; Tang, R.; Yan, B.; Vachet, R. W.; Rotello, V. M. The Interplay of Monolayer Structure and Serum Protein Interactions on the Cellular Uptake of Gold Nanoparticles. *Small* **2012**, *8*, 2659–2663.
65. Zhu, Z.-J.; Ghosh, P. S.; Miranda, O. R.; Vachet, R. W.; Rotello, V. M. Multiplexed Screening of Cellular Uptake of Gold Nanoparticles Using Laser Desorption/Ionization Mass Spectrometry. *J. Am. Chem. Soc.* **2008**, *130*, 14139–14143.
66. Gessner, A.; Waicz, R.; Lieske, A.; Paulke, B. R.; Mäder, K.; Müller, R. H. Nanoparticles with Decreasing Surface Hydrophobicities: Influence on Plasma Protein Adsorption. *Int. J. Pharm.* **2000**, *196*, 245–249.
67. Baier, G.; Costa, C.; Zeller, A.; Baumann, D.; Sayer, C.; Araujo, P. H. H.; Mailänder, V.; Musyanovych, A.; Landfester, K. Bsa Adsorption on Differently Charged Polystyrene Nanoparticles Using Isothermal Titration Calorimetry and the Influence on Cellular Uptake. *Macromol. Biosci.* **2011**, *11*, 628–638.
68. Hühn, D.; Kantner, K.; Geidel, C.; Brandholt, S.; De Cock, I.; Soenen, S. J. H.; Rivera Gil, P.; Montenegro, J.-M.; Braeckmans, K.; Müllen, K.; Nienhaus, G. U.; Klapper, M.; Parak, W. J. Polymer-Coated Nanoparticles Interacting with Proteins and Cells: Focusing on the Sign of the Net Charge. *ACS Nano* **2013**, *7*, 3253–3263.
69. Fleischer, C. C.; Kumar, U.; Payne, C. K. Cellular Binding of Anionic Nanoparticles Is Inhibited by Serum Proteins Independent of Nanoparticle Composition. *Biomater. Sci.* **2013**, *1*, 975–982.
70. Lesniak, A.; Fenaroli, F.; Monopoli, M. P.; Åberg, C.; Dawson, K. A.; Salvati, A. Effects of the Presence or Absence of a Protein Corona on Silica Nanoparticle Uptake and Impact on Cells. *ACS Nano* **2012**, *6*, 5845–5857.
71. Yang, S. K.; Shi, X.; Park, S.; Doganay, S.; Ha, T.; Zimmerman, S. C. Monovalent, Clickable, Uncharged, Water-Soluble Perylenediimide-Cored Dendrimers for Target-Specific Fluorescent Biolabeling. *J. Am. Chem. Soc.* **2011**, *133*, 9964–9967.
72. Yang, S. K.; Zimmerman, S. C. Polyglycerol-Dendronized Perylenediimides as Stable, Water-Soluble Fluorophores. *Adv. Funct. Mater.* **2012**, *22*, 3023–3028.
73. Silverstein, S. C.; Steinman, R. M.; Cohn, Z. A. Endocytosis. *Annu. Rev. Biochem.* **1977**, *46*, 669–722.
74. Schmid, S. L.; Carter, L. L. Atp Is Required for Receptor-Mediated Endocytosis in Intact-Cells. *J. Cell Biol.* **1990**, *111*, 2307–2318.
75. Kam, N. W. S.; Liu, Z. A.; Dai, H. J. Carbon Nanotubes as Intracellular Transporters for Proteins and DNA: An Investigation of the Uptake Mechanism and Pathway. *Angew. Chem., Int. Ed.* **2006**, *45*, 577–581.
76. Chithrani, B. D.; Chan, W. C. W. Elucidating the Mechanism of Cellular Uptake and Removal of Protein-Coated Gold Nanoparticles of Different Sizes and Shapes. *Nano Lett.* **2007**, *7*, 1542–1550.
77. Kelly, P. M.; Åberg, C.; Polo, E.; O'Connell, A.; Cookman, J.; Fallon, J.; KrpetićŽeljka; Dawson, K. A. Mapping Protein Binding Sites on the Biomolecular Corona of Nanoparticles. *Nat. Nanotechnol.* **2015**, *10*, 472–479.
78. Valkó, K. Application of High-Performance Liquid Chromatography Based Measurements of Lipophilicity to Model Biological Distribution. *J. Chromatogr. A* **2004**, *1037*, 299–310.